LETTER

doi:10.1038/nature20120

Reorientation and faulting of Pluto due to volatile loading within Sputnik Planitia

James T. Keane[1], Isamu Matsuyama[1], Shunichi Kamata[2] & Jordan K. Steckloff[3,4]

Pluto is an astoundingly diverse, geologically dynamic world. The dominant feature is Sputnik Planitia—a tear-drop-shaped topographic depression approximately 1,000 kilometres in diameter possibly representing an ancient impact basin[1,2]. The interior of Sputnik Planitia is characterized by a smooth, craterless plain three to four kilometres beneath the surrounding rugged uplands, and represents the surface of a massive unit of actively convecting volatile ices (N_2, CH_4 and CO) several kilometres thick[1–5]. This large feature is very near the Pluto–Charon tidal axis. Here we report that the location of Sputnik Planitia is the natural consequence of the sequestration of volatile ices within the basin and the resulting reorientation (true polar wander) of Pluto. Loading of volatile ices within a basin the size of Sputnik Planitia can substantially alter Pluto's inertia tensor, resulting in a reorientation of the dwarf planet of around 60 degrees with respect to the rotational and tidal axes. The combination of this reorientation, loading and global expansion due to the freezing of a possible subsurface ocean generates stresses within the planet's lithosphere, resulting in a global network of extensional faults that closely replicate the observed fault networks on Pluto. Sputnik Planitia probably formed northwest of its present location, and was loaded with volatiles over million-year timescales as a result of volatile transport cycles on Pluto[6,7]. Pluto's past, present and future orientation is controlled by feedbacks between volatile sublimation and condensation, changing insolation conditions and Pluto's interior structure.

Centred at 176° E, 24° N, Sputnik Planitia is close to the Pluto–Charon tidal axis (Fig. 1). The alignment of large geologic features with the principal axes of inertia is the hallmark of true polar wander[8] (TPW). In a minimum energy state, planets align their minimum (maximum) principal axis of inertia with the tidal (spin) axis. TPW occurs when mass is redistributed within the planet and the geographic locations of these axes change. To remain in a minimum energy state, the planet reorients to realign these principal axes with the tidal/spin axes. Notable examples of planetary TPW include: the reorientation of Enceladus to place the plume-producing tiger stripes at the south pole[9,10]; the reorientation of Mars to place the Tharsis volcanic rise at the equator[11]; and the reorientation of the Moon to place the South Pole–Aitken impact basin near the south pole[12] (see ref. 8 for a review). How a planet reorients is controlled by the feature's mass anomaly, Q', which is quantified in terms of degree-2 gravity coefficients: $Q' = -J_2^{SP*}/J_2^{RF}$ (where J_2^{SP*} is the degree-2 zonal spherical harmonic gravity coefficient of Sputnik Planitia when centred at Pluto's north pole and J_2^{RF} is the degree-2 zonal spherical harmonic gravity coefficient of Pluto's remnant figure; Methods). In the absence of a remnant figure, positive (negative) mass anomalies will reorient the planet to align with the tidal (spin) axis. The proximity of Sputnik Planitia to Pluto's tidal axis suggests that it is a positive mass anomaly.

TPW is counteracted by the planet's non-hydrostatic, elastically supported tidal-rotational bulge, which can preserve a previous tidal-rotational potential—a remnant figure. At present, no bulge (remnant or otherwise) has been observed at Pluto[13]. In the absence of measurements of Pluto's figure, we constructed a four-layer model of Pluto using viscoelastic Love number theory[14], using Pluto's mass and radius as constraints. Our nominal Pluto model consists of a silicate-rich core and a liquid water ocean overlaid by an H_2O-rich weak crust and elastic lithosphere (Methods).

Using our Pluto model, we evaluate how Pluto would reorient in response to the formation of Sputnik Planitia. The mass anomaly of Sputnik Planitia depends on its presumed density structure. Although topographic depressions are negative mass anomalies, impact basins (as Sputnik Planitia is hypothesized to be on the basis of its quasi-circular shape[2]) have stochastic mass anomalies owing to the complicated density structures that formed during the impact process[12,15] (Extended Data Fig. 1). Unavoidable impact basin components, such as ejecta blankets, can substantially offset the negative mass anomaly of the topographic depression (Extended Data Figs 2, 3). We remain agnostic as to the true structure of the Sputnik Planitia basin, and provide relationships that link Q' to the thickness of ice within the basin for several different simple basin structures (Fig. 2b–e, Extended Data Figs 1–3, Methods).

With these assumptions, we determined the possible initial locations of Sputnik Planitia as a function of Q'. We self-consistently adjusted Q' to account for the flexural response of Pluto's elastic lithosphere,

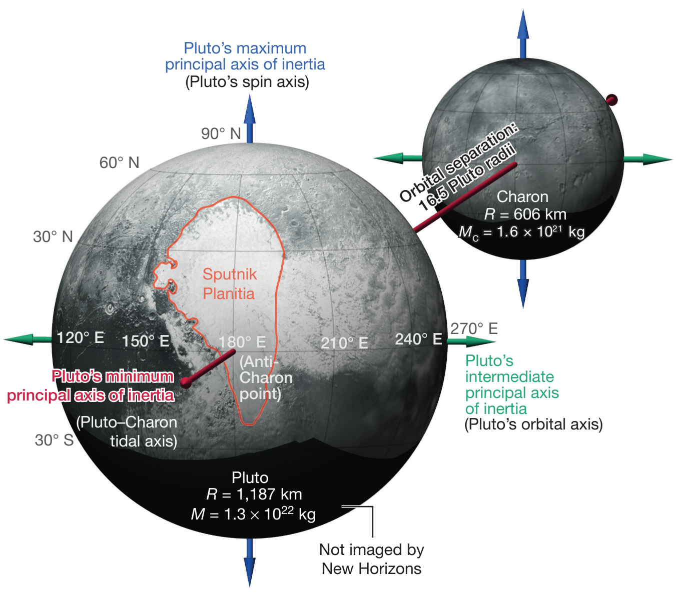

Figure 1 | Geometry of Sputnik Planitia in the Pluto–Charon system. Orthographic spherical projections of Pluto and Charon (to scale), with Sputnik Planitia and the principal axes of inertia labelled. Base map: NASA/Johns Hopkins University Applied Physics Laboratory/Southwest Research Institute.

[1]Lunar and Planetary Laboratory, Department of Planetary Science, University of Arizona, Tucson, Arizona 85721, USA. [2]Creative Research Institution, Hokkaido University, Sapporo, Japan. [3]Purdue University, Department of Earth, Atmospheric, and Planetary Sciences, West Lafayette, Indiana 47907, USA. [4]Planetary Science Institute, Tucson, Arizona 85719, USA.

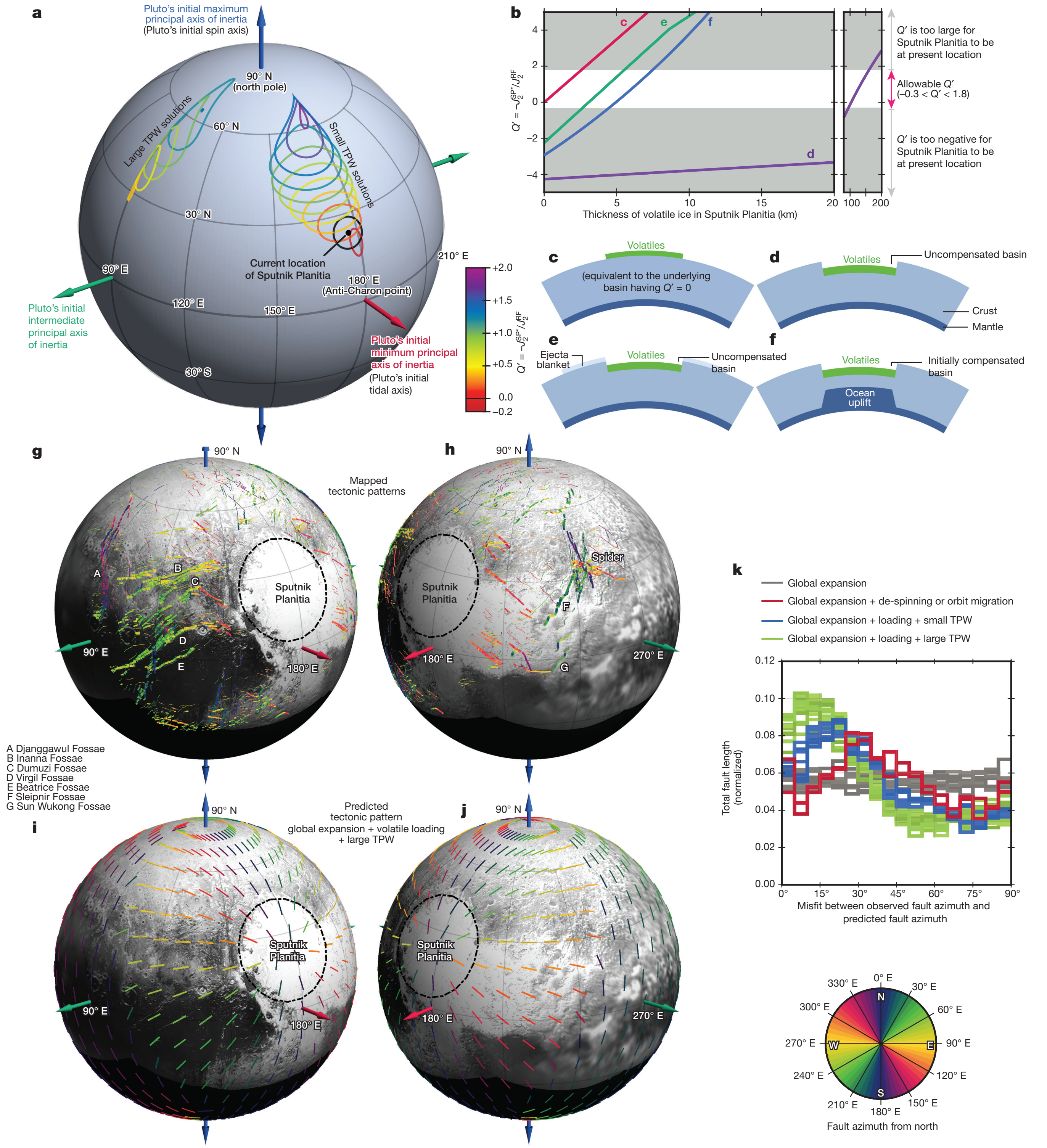

Figure 2 | True polar wander solutions for Sputnik Planitia and the resulting tectonic patterns. a, The possible initial locations of Sputnik Planitia before reorientation with respect to the principal axes of the remnant figure, as a function of Q'. **b**–**f**, Q' as a function of volatile thickness (**b**) for four idealized models of Sputnik Planitia (**c**–**f**). **c**, Volatiles on the surface (equivalent to volatiles loading a basin with $Q' = 0$). **d**, Volatiles filling an uncompensated basin. **e**, Volatiles filling an uncompensated impact basin surrounded by an ejecta blanket. **f**, Volatiles filling an impact basin that was initially compensated by an uplift in the subsurface ocean[16]. **g**, **h**, Tectonic features mapped in publicly available New Horizons imagery. Base map: NASA/Johns Hopkins University Applied Physics Laboratory/Southwest Research Institute. Faults are coloured by azimuth, and the line width corresponds to our certainty in the nature of fault: thick (thin) lines are unambiguously (possible) faults. **i**, **j**, Best-fitting predicted tectonic pattern resulting from global expansion, loading and a large TPW event. **k**, Binned misfit between observed and predicted fault azimuths (following the procedure used in ref. 19). Each line represents a different tectonic model (Extended Data Fig. 5; Methods). Large TPW solutions provide the best match to the observed distribution of faults.

which effectively increases the ice thickness that is required to produce a given reorientation. We performed a parameter space search—placing models of Sputnik Planitia with varying Q' values across the entire surface of Pluto and evaluating how Pluto reoriented in response. Contours in Fig. 2a bound the initial locations of Sputnik Planitia (as a function of Q') that reoriented Pluto to place Sputnik Planitia within 5° of its present location. Several key observations can be made from this figure. First, Sputnik Planitia could not have formed in any random location; the initial positions are limited to regions of a single quadrant of the northern, anti-Charon side of Pluto. This arises from energy constraints during single-episode TPW that prohibit the perturbing anomaly from crossing latitude and longitude lines of the remnant figure's principal axes. Within this quadrant, the available initial conditions are further constrained, as Sputnik Planitia is not exactly at the tidal axis. Second, the parameter space overwhelmingly favours positive Q' values (Extended Data Fig. 4). Q' is constrained to be between -0.3 and 1.8. This reveals that Sputnik Planitia is not a purely uncompensated topographic depression, as such a feature would have $Q' = -4$ (Fig. 2b, d), which would completely overwhelm Pluto's remnant figure and reorient Sputnik Planitia to the north pole. Ices alone are not sufficient to cancel out this negative anomaly, as it would require an untenable volume of ice within Sputnik Planitia (>100 km; Fig. 2b, d). Instead, some combination of ice and basin structure (for example, an ejecta blanket (Fig. 2b, e) or uplift of the subsurface ocean[16] (Fig. 2b, f)) is required for Sputnik Planitia to be at its present location. Third, depending on the presumed structure of Sputnik Planitia, the required ice thicknesses range from 0 to 10 km (Fig. 2b–f, Extended Data Fig. 3, Methods), which is consistent with previous estimates of ice thickness within Sputnik Planitia that are based on inferences of basin geometry[2], isostasy of mountain-sized H_2O icebergs floating in Sputnik Planitia, and modelling of solid-state convection of ice within Sputnik Planitia[4,5]. Finally, there are two families of TPW solutions: 'large' solutions, where Sputnik Planitia started northwest of its present location; and 'small' solutions, where Sputnik Planitia started north of its present location (Extended Data Fig. 4a, b). Large TPW solutions occur when the intermediate and minimum principal axes of inertia swap (hence the minimum Q' value for large TPW solutions, which are related to the moment differences).

As a planet reorients, each surface location experiences a change in the tidal rotational potential. This builds stress in the lithosphere, eventually resulting in faults with a characteristic global pattern[17]. Pluto possesses a global non-random system of extensional faults[1,2] (Fig. 2g, h). The lack of observed compressional or translational faults probably reflects global expansion due to the freezing of a subsurface ocean[18]. Using our initial locations of Sputnik Planitia (Fig. 2a), we calculated the tectonic patterns for a range of possible TPW scenarios, including the effects of reorientation, global expansion and loading of ice within Sputnik Planitia (Methods). Figure 2i, j shows our best-fitting TPW solution. Proximal to Sputnik Planitia, faults are quasi-radial, primarily from loading stresses. Distal to Sputnik Planitia, TPW stresses dominate and the orientations of the faults change. The predicted tectonic patterns are not strongly sensitive to the bulk properties of Pluto, but are sensitive to the initial location, size and thickness of ice within Sputnik Planitia (Extended Data Fig. 5). We quantified how well our predicted fault geometries fit by

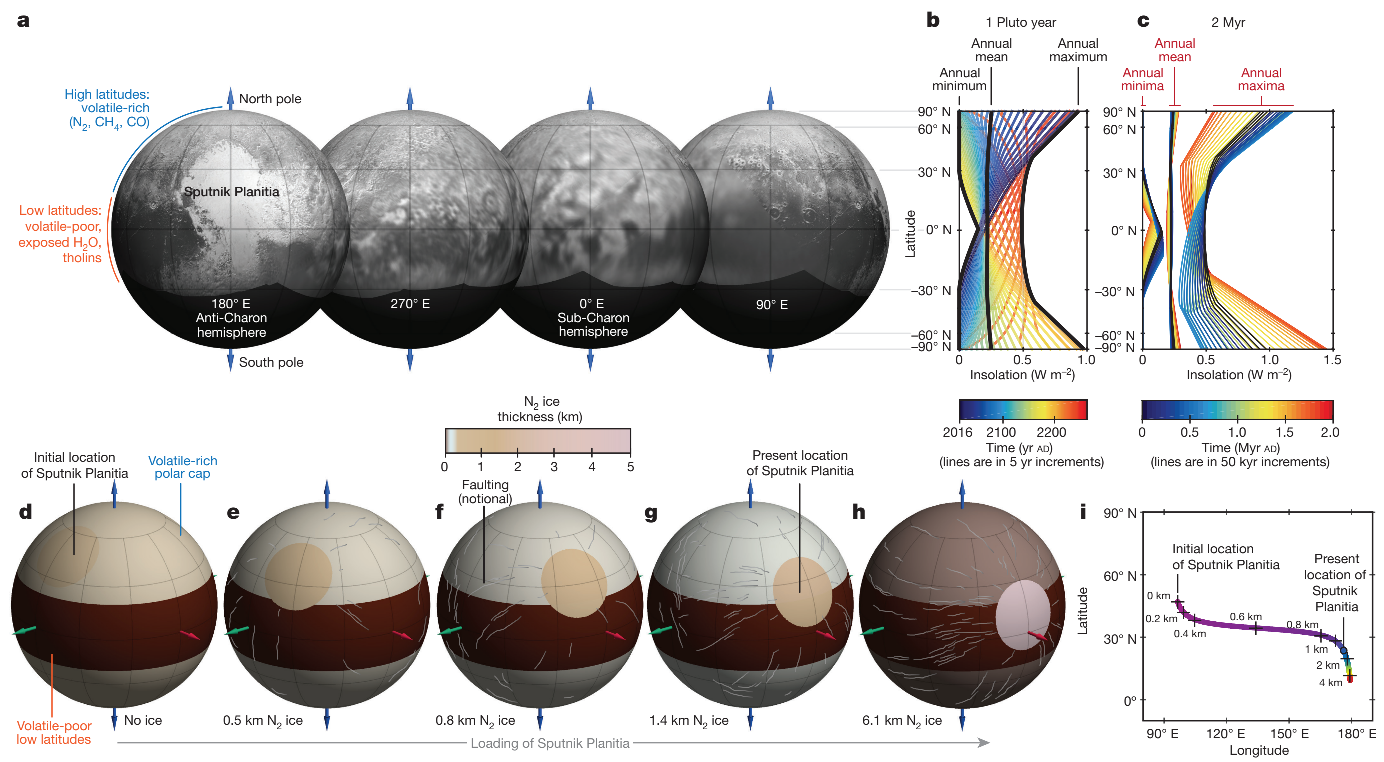

Figure 3 | Insolation patterns and volatile-driven TPW of Pluto. **a**, Orthographic spherical projection of Pluto, highlighting the latitudinal trends in albedo and volatile content. Base map: NASA/Johns Hopkins University Applied Physics Laboratory/Southwest Research Institute. **b**, Insolation as a function of time on Pluto. Coloured lines denote average insolation over one Pluto day; black lines denote the minimum, maximum and mean over one Pluto year. **c**, Variations in annual minima, maxima and mean insolation over 2 Myr. **d**–**h**, A simple model of our proposed volatile-induced reorientation of Pluto, where an equivalent global layer of 200 m of volatile ice is transferred from the poles to Sputnik Planitia (assuming the underlying basin has $Q' = 0$, as in Fig. 2b, c) for various ice loadings from 0 km to 6.1 km in thickness. Sputnik Planitia initially formed at higher latitude, northwest of its present location. As volatiles migrate into Sputnik Planitia from other cold traps, Pluto reorients and fractures (see Extended Data Fig. 6, Supplementary Videos 1–3 and Methods). **i**, The latitude and longitude of Sputnik Planitia are shown as a function of the thickness of ice within the basin. If volatiles continue to migrate into Sputnik Planitia, Pluto will continue to reorient towards the tidal axis.

measuring the difference between the observed and predicted fault azimuths[19] (Fig. 2k). Large TPW solutions yielded the best fit to the observed fault distribution and are marginally better than small TPW solutions. The observed fault geometry is inconsistent with global expansion, de-spinning or orbit migration[20] alone (Extended Data Fig. 5). We do not accurately predict the locations of the Sun Wukong Fossae (SWF) and 'spider' fault network east of Sputnik Planitia. Although our model does predict the confluence of eastward- and northward-trending faults at some distance from Sputnik Planitia (as demonstrated by the accurate fitting of faults west of Sputnik Planitia), the SWF and 'spider' are westward of the predicted eastern transition. This difference may be due to oversimplifications in our model geometry of Sputnik Planitia, inhomogeneity in the lithosphere, or faulting during different stress conditions (Extended Data Fig. 6). Nonetheless, TPW, loading and global expansion provide the most comprehensive single explanation for the global pattern of faults on Pluto.

If ice loading within Sputnik Planitia drove TPW, then this suggests a feedback between the planet's volatile cycle and rotational stability. Such a feedback was previously discounted on the basis of Pluto's insolation geometry[21]. Pluto's large obliquity (122°) means that the equator receives less insolation than the poles[22] (Fig. 3b, c). Therefore, one might expect volatiles to accumulate at Pluto's equator, building a stabilizing equatorial bulge and inhibiting TPW[21]. However, while Pluto's equator receives less insolation, it is never the coldest part of the planet (Fig. 3b, c). Pluto's poles oscillate seasonally between long polar nights, and if volatiles are sufficiently mobile the poles may still be the preferred sites for volatile deposition[7,23]. This may explain why volatiles are found preferentially at higher latitudes on Pluto[3] (Fig. 3a). Our TPW solutions suggest that Sputnik Planitia formed at higher latitudes in these regions of enhanced seasonal volatile deposition. We posit that Sputnik Planitia is a cold trap (see Methods), and over time it accreted a large fraction of Pluto's volatile reservoir, driving reorientation (Fig. 3d–h). The final location of Sputnik Planitia is set by Pluto's total volatile reservoir, the remnant figure and the feedback between TPW and volatile stability within Sputnik Planitia. The proximity of Sputnik Planitia to the latitude of minimum mean insolation[24] (Fig. 3b) may be evidence that a TPW–volatile stability feedback is active. If volatiles migrate into and out of Sputnik Planitia on seasonal timescales, then Pluto may experience small-amplitude wobbles akin to Earth's annual, atmospheric-pressure-driven wobbles[25] (see Methods). Similar volatile-driven reorientation feedbacks may be important for continued geologic activity on other large Kuiper belt objects and planetary bodies with large reservoirs of mobile volatiles.

Online Content Methods, along with any additional Extended Data display items and Source Data, are available in the online version of the paper; references unique to these sections appear only in the online paper.

Received 17 May; accepted 26 September 2016.
Published online 16 November 2016.

1. Stern, S. A. *et al.* The Pluto system: initial results from its exploration by New Horizons. *Science* **350,** aad1815 (2015).
2. Moore, J. M. *et al.* The geology of Pluto and Charon through the eyes of New Horizons. *Science* **351,** 1284–1293 (2016).
3. Grundy, W. M. *et al.* Surface compositions across Pluto and Charon. *Science* **351,** aad9189 (2016).
4. McKinnon, W. B. *et al.* Convection in a volatile nitrogen-ice-rich layer drives Pluto's geological vigour. *Nature* **534,** 82–85 (2016).
5. Trowbridge, A. J. *et al.* Vigorous convection as the explanation for Pluto's polygonal terrain. *Nature* **534,** 79–81 (2016).
6. Binzel, R. P. Long term variations of a volatile methane reservoir on Pluto. In *21st Lunar Planet. Sci. Conf.* 87–88 (Lunar and Planetary Institute, 1990).
7. Spencer, J. R. *et al.* in *Pluto and Charon* (eds Stern, S. A. & Tholen, D. J.) 435–474 (Univ. Arizona Press, 1997).
8. Matsuyama, I., Nimmo, F. & Mitrovica, J. X. Planetary reorientation. *Annu. Rev. Earth Planet. Sci.* **42,** 605–634 (2014).
9. Nimmo, F. & Pappalardo, R. T. Diapir-induced reorientation of Saturn's moon Enceladus. *Nature* **441,** 614–616 (2006).
10. Collins, G. C. & Goodman, J. C. Enceladus' south polar sea. *Icarus* **189,** 72–82 (2007).
11. Perron, J. T., Mitrovica, J. X., Manga, M., Matsuyama, I. & Richards, M. A. Evidence for an ancient Martian ocean in the topography of deformed shorelines. *Nature* **447,** 840–843 (2007).
12. Keane, J. T. & Matsuyama, I. Evidence for lunar true polar wander and a past low eccentricity, synchronous lunar orbit. *Geophys. Res. Lett.* **41,** 6610–6619 (2014).
13. Nimmo, F. *et al.* Mean radius and shape of Pluto and Charon from New Horizons images. *Icarus* http://dx.doi.org/10.1016/j.icarus.2016.06.027 (2016).
14. Peltier, W. R. The impulse response of a Maxwell Earth. *Rev. Geophys. Space Phys.* **12,** 649–669 (1974).
15. Melosh, H. J. *et al.* The origin of lunar mascon basins. *Science* **340,** 1552–1555 (2013).
16. Nimmo, F. *et al.* Reorientation of Sputnik Planitia implies a subsurface ocean on Pluto. *Nature* http://dx.doi.org/10.1038/nature20148 (2016).
17. Matsuyama, I. & Nimmo, F. Tectonic patterns on reoriented and despun planetary bodies. *Icarus* **195,** 459–473 (2008).
18. Hammond, N. P., Barr, A. C. & Parmentier, E. M. Recent tectonic activity on Pluto driven by phase changes in the ice shell. *Geophys. Res. Lett.* **43,** 6775–6782 (2016).
19. Watters, T. R. *et al.* Global thrust faulting on the Moon and the influence of tidal stresses. *Geology* **43,** 851–854 (2015).
20. Matsuyama, I. & Nimmo, F. Pluto's tectonic pattern predictions. In *44th Lunar Planet. Sci. Conf.* 1399 (Lunar and Planetary Institute, 2013).
21. Rubincam, D. P. Polar wander on Triton and Pluto due to volatile migration. *Icarus* **163,** 469–478 (2003).
22. Earle, A. M. & Binzel, R. P. Pluto's insolation history: latitudinal variations and effects on atmospheric pressure. *Icarus* **250,** 405–412 (2015).
23. Hansen, C. J., Paige, D. A. & Young, L. A. Pluto's climate modeled with new observational constraints. *Icarus* **246,** 183–191 (2015).
24. Hamilton, D. P. *et al.* The rapid formation of Sputnik Planitia early in Pluto's history. *Nature* (in the press).
25. Gross, R. S., Fukumori, I. & Menemenlis, D. Atmospheric and oceanic excitation of the Earth's wobbles during 1980–2000. *J. Geophys. Res.* **108,** 2370 (2003).

Supplementary Information is available in the online version of the paper.

Acknowledgements We thank the New Horizons science team for their many years of work that resulted in the successful flyby of Pluto, and for promptly releasing the public data and published work[1–4,13,16] that enabled this research. We note that all names of features on Pluto are informal. J.T.K. acknowledges support from the University of Arizona Theoretical Astrophysics Program and NASA Solar System Workings.

Author Contributions J.T.K. identified the link between Sputnik Planitia and the tidal axis, performed true polar wander analyses, mapping and analysis of tectonic features, proposed connection between polar wander and secular volatile transport, was the primary author of the text and created all figures. I.M. performed analyses of Pluto's shape and gravity field and performed tectonics calculations. S.K. provided Love numbers for Pluto. J.K.S. provided estimates of volatile deposition timescales for Sputnik Planitia and provided input on volatile transport.

Author Information Reprints and permissions information is available at www.nature.com/reprints. The authors declare no competing financial interests. Readers are welcome to comment on the online version of the paper. Correspondence and requests for materials should be addressed to J.T.K. (jkeane@lpl.arizona.edu).

METHODS

Could Sputnik Planitia be at the tidal axis by chance? To assess whether the alignment of Sputnik Planitia and the tidal axis is due to chance, we generated a large number ($N > 100{,}000$) of points on the surface of a unit sphere. The latitude, θ, and longitude, φ, of a randomly positioned point on a sphere can be written as $\theta = \cos^{-1}(2u - 1)$ and $\varphi = 2\pi v$, where u and v are random numbers spanning 0 and 1. We calculated the great-circle distance between each individual random point and the three nearest surface expressions of the three principal axes of inertia. Extended Data Fig. 7 shows the cumulative probability of a point being a certain angular distance away from one particular principal axis (for example, the tidal axis) in blue. The cumulative probability of a point being near one of two particular principal axes (for example, the tidal or spin axes) is orange. The cumulative probability of a point being near any one of the three principal axes is yellow. A simpler geometric method for calculating the probability of Sputnik Planitia being within angular distance, γ, of any single principal axis (blue line in Extended Data Fig. 7) involves taking the ratio of the area of two spherical caps with radius γ to the total surface area of the sphere. With this method, the probability is simply $1 - \cos(\gamma)$.

We determined the centre of Sputnik Planitia by fitting it to a small circle using the available global map of Pluto (Fig. 1). Using this technique, we found a centre of 176° E, 24° N, which is around 24° away from the tidal axis. There is a probability of about 9% that Sputnik Planitia is this close to the tidal axis (either at the anti-Charon point or at the sub-Charon point), and an approximately 26% chance that Sputnik Planitia would be close to any one of the principal axes. The authors of ref. 16 fitted Sputnik Planitia to an ellipse, and found a centre closer to the tidal axis, resulting in correspondingly smaller probabilities.

Predicted shape and gravity field of Pluto. We follow the notation of ref. 8, and describe Pluto's gravity field and shape in terms of spherical harmonic coefficients. However, an important correction must be made when investigating the tidal deformation of Pluto due to Charon. It is normally assumed that the perturbing body has a mass that is much larger than that of the deforming body (for example, Jupiter is much more massive than Europa). However, if the mass of the perturbing body is comparable to, or smaller than, the mass of the larger body (as is the case for Charon acting on Pluto), many of the gravity and shape equations must be augmented.

Ignoring TPW, the hydrostatic, non-zero degree-2 spherical harmonic gravity coefficients, $C_{2,0}$ (also commonly written as J_2) and $C_{2,2}$, can be written as:

$$J_2^{\mathrm{HYD}} = -C_{2,0}^{\mathrm{HYD}} = \frac{1}{6} k_2^{\mathrm{T}'} q \left(\frac{2M + 5M_{\mathrm{C}}}{M + M_{\mathrm{C}}} \right)$$

$$C_{2,2}^{\mathrm{HYD}} = \frac{1}{4} k_2^{\mathrm{T}'} q \left(\frac{M_{\mathrm{C}}}{M + M_{\mathrm{C}}} \right)$$

where q is defined as $q \equiv (\Omega^2 R^3)/(GM)$, Ω is the rotation rate of Pluto/Charon, M is the mass of Pluto, M_{C} is the mass of Charon, G is the gravitational constant and $k_2^{\mathrm{T}'}$ is the degree-2 long-term tidal Love number for the case without an elastic lithosphere. Love numbers (potential Love number k_2 and displacement Love numbers h_2 and ℓ_2) describe the response of a planet to the perturbing potential. Ignoring any contribution from TPW:

$$\frac{J_2^{\mathrm{HYD}}}{C_{2,2}^{\mathrm{HYD}}} = \frac{2}{3} \left(\frac{2M + 5M_{\mathrm{C}}}{M_{\mathrm{C}}} \right)$$

Note that this ratio is independent of the interior structure, and if $M_{\mathrm{C}} \gg M$ (as is commonly assumed for tidally deformed planetary satellites) then $J_2^{\mathrm{HYD}}/C_{2,2}^{\mathrm{HYD}} = 10/3 = 3.3$. For Pluto, $J_2^{\mathrm{HYD}}/C_{2,2}^{\mathrm{HYD}} = 14.3$.

Ignoring TPW, the radial displacement due to hydrostatic rotational and tidal deformation can be written:

$$d_r(\theta, \varphi) = h_2^{\mathrm{T}'} R q \left[-\frac{1}{3} P_{2,0}(\cos\theta) - \frac{1}{2} \left(\frac{M_{\mathrm{C}}}{M + M_{\mathrm{C}}} \right) P_{2,0}(\cos\theta) + \frac{1}{4} \left(\frac{M_{\mathrm{C}}}{M + M_{\mathrm{C}}} \right) P_{2,2}(\cos\theta)\cos(2\varphi) \right]$$

where R is the radius of Pluto, $h_2^{\mathrm{T}'}$ is the degree-2 long-term tidal displacement Love number for the case without an elastic lithosphere and $P_{2,0}$ is the degree-2 order-0 unnormalized associated Legendre function[26]. The corresponding oblateness for Pluto is:

$$\frac{d_r(\theta = 90°, \varphi = 0°) - d_r(\theta = 0°, \varphi = 0°)}{R + d_r(\theta = 90°, \varphi = 0°)} \approx \frac{d_r(\theta = 90°, \varphi = 0°) - d_r(\theta = 0°, \varphi = 0°)}{R} = 4.13 \times 10^{-4} \left(\frac{h_2^{\mathrm{T}'}}{5/2} \right)$$

For our nominal Pluto interior structure model, $h_2^{\mathrm{T}'} = 1.773$, and so the oblateness is 2.93×10^{-4}. The maximum possible oblateness would occur if Pluto were a uniform, hydrostatic fluid ($h_2^{\mathrm{T}'} = 5/2$), corresponding to an oblateness of 4.13×10^{-4}. The New Horizons upper limit for Pluto's oblateness is an order of magnitude larger than either of these values[13].

The inertia tensor of Pluto and TPW. TPW solutions can be found by diagonalizing the non-equilibrium inertia tensor. We follow ref. 8 to compute this inertia tensor, with the aforementioned modifications to account for the small M_{C} with respect to M. Ignoring the spherically symmetric contributions (which do not control orientation of a planet), the non-equilibrium inertia tensor can be written as:

$$I_{ij} = \left[\left(1 + k_2^{\mathrm{L}}\right) M R^2 C_{2,0}^{\mathrm{SP}*} \left(\frac{1}{3}\delta_{ij} - \hat{e}_i^{\mathrm{SP}} \hat{e}_j^{\mathrm{SP}} \right) \right] + \left[\left(k_2^{\mathrm{T}'} - k_2^{\mathrm{T}} \right) \frac{\Omega^2 R^5}{3G} \left(\hat{e}_i^{\mathrm{R}'} \hat{e}_j^{\mathrm{R}'} - \frac{1}{3}\delta_{ij} \right) \right] + \left[\left(k_2^{\mathrm{T}'} - k_2^{\mathrm{T}} \right) \left(\frac{M_{\mathrm{C}}}{M + M_{\mathrm{C}}} \right) \frac{\Omega^2 R^5}{G} \left(\frac{1}{3}\delta_{ij} - \hat{e}_i^{\mathrm{T}'} \hat{e}_j^{\mathrm{T}'} \right) \right]$$

where the first bracketed term is the contribution from loading in Sputnik Planitia, the second bracketed term is the rotational deformation and the final term is the tidal deformation. Together, the last two bracketed terms represent the rotational and tidal components of the remnant figure; δ_{ij} is the Kronecker delta function, and $\hat{\boldsymbol{e}}^{\mathrm{SP}}$, $\hat{\boldsymbol{e}}^{\mathrm{R}'}$ and $\hat{\boldsymbol{e}}^{\mathrm{T}'}$ are unit vectors describing the centre of Sputnik Planitia, the initial rotation pole and the initial tidal pole (sub-Charon point), respectively. For example, if the spherical coordinates of Sputnik Planitia are (θ_{SP}, φ_{SP}), then $\hat{\boldsymbol{e}}^{\mathrm{SP}} = (\sin\theta_{\mathrm{SP}}\cos\varphi_{\mathrm{SP}}, \sin\theta_{\mathrm{SP}}\sin\varphi_{\mathrm{SP}}, \cos\theta_{\mathrm{SP}})$. k_2^{L} is the degree-2 loading Love number. All Love numbers here are the long-term Love numbers, or so-called fluid Love numbers. $C_{2,0}^{\mathrm{SP}*}$ is the unnormalized degree-2 gravity coefficient of Sputnik Planitia for the case when it is centred at the north pole. Assuming an axisymmetric load with surface density σ and angular radius ψ:

$$C_{2,0}^{\mathrm{SP}*} = \frac{2\pi R^2 \sigma}{M} \int_0^{\psi} \mathrm{d}\theta \sin\theta P_{2,0}(\cos\theta)$$

where $J_2 \equiv -C_{2,0}$. Because the remnant figure provides stabilization against TPW, it is useful to define a normalized load size:

$$Q' = -\frac{C_{2,0}^{\mathrm{SP}*}}{C_{2,0}^{\mathrm{RF}}} = \frac{\left(1 + k_2^{\mathrm{L}}\right)}{\left(k_2^{\mathrm{T}'} - k_2^{\mathrm{T}}\right)} \frac{GM}{\Omega^2 R^3} \frac{6(M + M_{\mathrm{C}})}{(2M + 5M_{\mathrm{C}})} C_{2,0}^{\mathrm{SP}*}$$

where $C_{2,0}^{\mathrm{RF}}$ is the unnormalized degree-2 zonal gravity coefficient associated with Pluto's remnant figure, which can be derived from converting the inertia tensor of the remnant figure into spherical gravity coefficients[27]. Note that this normalization is different from the one used in refs 8 and 16 because it includes both the rotational and tidal deformation contributions to the remnant figure (hence our use of Q' instead of Q). Q' is related to Q by:

$$Q = \left(1 + \frac{3}{2} \frac{M_{\mathrm{C}}}{M + M_{\mathrm{C}}}\right) Q'$$

For the case of Pluto and Charon, the factor in front of Q' is 1.16. With this normalization, TPW solutions can be found by diagonalizing the normalized, non-equilibrium inertia tensor:

$$\bar{I}_{ij} = Q' \left(\frac{1}{3}\delta_{ij} - \hat{e}_i^{\mathrm{SP}} \hat{e}_j^{\mathrm{SP}} \right) + \frac{2(M + M_{\mathrm{C}})}{(2M + 5M_{\mathrm{C}})} \left(\hat{e}_i^{\mathrm{R}'} \hat{e}_j^{\mathrm{R}'} - \frac{1}{3}\delta_{ij} \right) + \frac{6M_{\mathrm{C}}}{(2M + 5M_{\mathrm{C}})} \left(\frac{1}{3}\delta_{ij} - \hat{e}_i^{\mathrm{T}'} \hat{e}_j^{\mathrm{T}'} \right)$$

The interior structure dependence is described by the Love numbers factor $\left(1 + k_2^{\mathrm{L}}\right)/\left(k_2^{\mathrm{T}'} - k_2^{\mathrm{T}}\right)$ in the definition of Q'. Both the numerator and denominator of this factor are sensitive to the interior structure, but this dependence almost disappears when the ratio is used. This is shown clearly in Extended Data Fig. 5k, and further enhances the robustness of our solutions.

We compute the long-term Love numbers by solving the mass, momentum and Poisson equations for the deformation of a spherically symmetric, non-rotating, elastic and isotropic body[14,28,29]. As discussed in the main text, we considered a four-layer interior structure model, consisting of a silicate-rich solid core (density: 3.36 g cm^{-3}; radius: 858 km), liquid water ocean (density: 1.0 g cm^{-3}; thickness: 10 km), overlaid by a two-layer water-ice mantle (density: 0.95 g cm^{-3}; thickness: 320 km). The ice mantle is comprised of a weak, viscous lower mantle, beneath an elastic lithosphere of varying elastic thickness (0–70 km), rigidity (3.49 GPa) and bulk modulus (9.3 GPa) (ref. 30). The long-term Love numbers can be computed by considering the infinite time limit. Alternatively, these Love numbers can be computed by assuming that all regions, with the exception of the elastic lithosphere, are inviscid. For simplicity, we assume infinite viscosity in all layers, zero frequency dependence and that only the upper mantle is elastic (all common assumptions). Love numbers decrease as the elastic thickness or rigidity of the lithosphere decrease. For our nominal interior structure with elastic thicknesses spanning 0 to 70 km, k_2^{T} spans 0.7653 to 0.4682; k_2^{L} spans −0.9856 to −0.4500. Similarly, the tidal displacement Love numbers, h_2 and ℓ_2, can be evaluated. Over the same span in elastic thickness, h_2^{T} spans 1.7509 to 0.9182; h_2^{L} spans −3.2230 to −1.7345; ℓ_2^{T} spans 0.4374 to 0.9182; and ℓ_2^{L} spans −0.7847 to −0.3858. Our Love numbers differ slightly from those of ref. 16, primarily owing to different assumptions about the core structure. Our results are not strongly sensitive to assumed Love numbers and interior structure.

Tectonics patterns due to global expansion, TPW and loading of Sputnik Planitia. Following ref. 30, the stresses on the surface of a planet due to a generalized displacement $\boldsymbol{d} = (d_r, d_\theta, d_\varphi)$ in spherical coordinates can be written:

$$\tau_{\theta\theta} = \frac{\lambda}{\lambda+2\mu}\tau_{rr} + \frac{2\mu}{R(\lambda+2\mu)}\left[(3\lambda+2\mu)d_r + 2(\lambda+\mu)\partial_\theta d_\theta + \lambda\left(\frac{\partial_\varphi d_\varphi}{\sin\theta} + d_\theta \cot\theta\right)\right]$$

$$\tau_{\varphi\varphi} = \frac{\lambda}{\lambda+2\mu}\tau_{rr} + \frac{2\mu}{R(\lambda+2\mu)}\left[(3\lambda+2\mu)d_r + \lambda\partial_\theta d_\theta + 2(\lambda+\mu)\left(\frac{\partial_\varphi d_\varphi}{\sin\theta} + d_\theta \cot\theta\right)\right]$$

$$\tau_{\theta\varphi} = \frac{\mu}{R}\left[\partial_\theta d_\varphi + \frac{\partial_\varphi d_\theta}{\sin\theta} - d_\varphi \cot\theta\right]$$

where we assume a compressible interior, and μ and λ are the Lamé parameters. Note that $\tau_{rr} = 0$ for displacements due to rotational or tidal deformation.

From the previous equations, the isotropic stress due to an isotropic radius change, δR, can be written as:

$$\tau_{\theta\theta} = \tau_{\varphi\varphi} = 2\mu\frac{(2\mu+3\lambda)}{(\lambda+2\mu)}\frac{\delta R}{R} = \frac{E}{(1-\nu)}\frac{\delta R}{R}$$

where E and ν are the elastic modulus and Poisson's ratio, respectively.

The displacement due to rotational and tidal deformation associated with TPW can be written as:

$$(d_r, d_\theta, d_\varphi) = R\sum_{m=0}^{l}\sum_{i=1}^{2}\left(h_2, \ell_2\partial_\theta, \frac{\ell_2\partial_\varphi}{\sin\theta}\right)\left(U_{2,m,i}^{\mathrm{f}} - U_{2,m,i}^{\mathrm{i}}\right)Y_{l,m,i}$$

where U^{i} and U^{f} are the initial (pre-TPW) and final (post-TPW) gravitational potentials, respectively. $Y_{l,m,i}$ are the spherical surface harmonics:

$$\begin{pmatrix} Y_{l,m,1}(\theta,\varphi) \\ Y_{l,m,2}(\theta,\varphi) \end{pmatrix} = P_{l,m}(\cos\theta)\begin{pmatrix} \cos m\varphi \\ \sin m\varphi \end{pmatrix}$$

where l and m are the spherical harmonic degree and order, respectively. The gravitational potential expansion coefficients are:

$$U_{2,m,i}^{\mathrm{f}} = (2-\delta_{m0})\frac{(2-m)!}{(2+m)!}\left[-\frac{\Omega_{\mathrm{f}}^2 R^3}{3GM}Y_{2,m,i}\left(\theta_{\mathrm{R}}^{\mathrm{f}}, \varphi_{\mathrm{R}}^{\mathrm{f}}\right) + \frac{M_{\mathrm{C}}}{M+M_{\mathrm{C}}}\frac{\Omega_{\mathrm{f}}^2 R^3}{GM}Y_{2,m,i}\left(\theta_{\mathrm{T}}^{\mathrm{f}}, \varphi_{\mathrm{T}}^{\mathrm{f}}\right)\right]$$

$$U_{2,m,i}^{\mathrm{i}} = (2-\delta_{m0})\frac{(2-m)!}{(2+m)!}\left[-\frac{\Omega_{\mathrm{i}}^2 R^3}{3GM}Y_{2,m,i}\left(\theta_{\mathrm{R}}^{\mathrm{i}}, \varphi_{\mathrm{R}}^{\mathrm{i}}\right) + \frac{M_{\mathrm{C}}}{M+M_{\mathrm{C}}}\frac{\Omega_{\mathrm{i}}^2 R^3}{GM}Y_{2,m,i}\left(\theta_{\mathrm{T}}^{\mathrm{i}}, \varphi_{\mathrm{T}}^{\mathrm{i}}\right)\right]$$

where $(\theta_{\mathrm{R}}^{\mathrm{f}}, \varphi_{\mathrm{R}}^{\mathrm{f}})$ and $(\theta_{\mathrm{T}}^{\mathrm{f}}, \varphi_{\mathrm{T}}^{\mathrm{f}})$ are the spherical coordinates of the final rotation pole and the tidal pole (sub-Charon point), respectively. $(\theta_{\mathrm{R}}^{\mathrm{i}}, \varphi_{\mathrm{R}}^{\mathrm{i}})$ and $(\theta_{\mathrm{T}}^{\mathrm{i}}, \varphi_{\mathrm{T}}^{\mathrm{i}})$ are the spherical coordinates of the initial rotation pole and tidal pole (sub-Charon point). Ω_{i} and Ω_{f} are the initial and final rotation rates.

The displacement due to mass loading in Sputnik Planitia can be written as:

$$(d_r, d_\theta, d_\varphi) = R\sum_{l=0}^{\infty}\sum_{m=0}^{l}\sum_{i=1}^{2}\left(h_l^{\mathrm{L}}, \ell_l^{\mathrm{L}}\partial_\theta, \frac{\ell_l^{\mathrm{L}}\partial_\varphi}{\sin\theta}\right)U_{l,m,i}$$

Assuming an axisymmetric load, the gravitational potential expansion coefficients are:

$$U_{l,m,i} = (2-\delta_{m0})\frac{(2-m)!}{(2+m)!}\frac{2\pi R^2\sigma}{M}Y_{l,m,i}(\theta_{\mathrm{SP}}, \varphi_{\mathrm{SP}})\int_0^{\psi} \mathrm{d}\theta \sin\theta \mathrm{P}_{l,0}(\cos\theta)$$

and the radial stress due to mass loading in Sputnik Planitia can be written as:

$$\tau_{rr} = -\frac{gM}{4\pi R^2}\sum_{l=0}^{\infty}\sum_{m=0}^{l}\sum_{i=1}^{2}(2l+1)U_{l,m,i}Y_{l,m,i}(\theta_{\mathrm{SP}}, \varphi_{\mathrm{SP}})$$

where g is the surface gravity of Pluto ($g = GM/R^2$).

Tectonics patterns are derived from the eigenvalue of the local stress tensor[31], which can be constructed by summing all stress components mentioned above. Normal faulting is perpendicular to the maximum principal stress.

Rotational stability of Pluto. If volatiles tend to accumulate at Pluto's north and south poles, this may make Pluto more susceptible to polar wander than previously expected[21]. As a polar ice cap grows in mass, it effectively reduces the dynamical flattening of the planet. Once the polar caps exceed the tidal rotational flattening, the maximum and intermediate principal axes of inertia will swap—reorienting Pluto by 90° around the tidal axis, placing the former polar cap on the intermediate principal axis of inertia (the orbital axis at (90° E, 0° N) or (270° E, 0° N) as in Fig. 1). If we assume that volatiles are sequestered into two 60°-radius polar caps, with ice densities of 1 g cm^{-3}, then this rotational stability limit occurs when the ice caps reach a thickness of around 180 m (equivalent to a global layer of around 90 m). This calculation assumes that the polar ice caps can be partially compensated by lithospheric flexure. If caps are not partially supported (or if they are constructed more rapidly than the lithosphere can adjust), then the threshold is smaller: about 80 m (equivalent to a global layer of about 40 m). Note that the total volume of ice required within these 'destabilizing' ice caps is comparable to the expected volume of volatile ice within Sputnik Planitia.

If polar ice caps can grow large enough to destabilize Pluto, they would result in substantially different tectonic patterns—perhaps akin to 'crop-circle' faults on Europa, which are hypothesized to result from a similar style of reorientation[32] (albeit due to differential crustal thickening, and not surface volatile transport). The lack of such an observed tectonic pattern may suggest that this style of reorientation has not occurred on Pluto. Perhaps the volatile reservoir on Pluto is too small to build such a polar cap, or the remnant figure is larger. Although Pluto's polar regions are indeed rich in volatiles[3], the thickness of volatiles and their compensation state are unclear. Some eroded mantled terrains in the northern uplands have thicknesses of approximately 1 km (ref. 2). If these deposits ever covered large fractions of polar regions, they would easily destabilize Pluto. If polar volatiles are sufficiently mobile, then it is conceivable that they may adjust to changes in the planet's insolation conditions faster than the planet can reorient. In such a case, polar volatiles would act more similarly to a hydrostatic tidal rotational bulge, and may not be capable of controlling the planet's orientation over long timescales.

Sputnik Planitia as a cold trap. As Sputnik Planitia is a large topographic low, and there is no observed troposphere on Pluto[33] (that is, temperature decreases with altitude on Pluto), we posit that Sputnik Planitia is an intrinsic cold trap. Other factors may contribute to Sputnik Planitia being a cold trap, such as atmospheric circulation in response to its topography or intrinsic albedo variations associated with the underlying basin. This hypothesis is explored in detail in ref. 34. Over time, scattered volatile ice deposits should migrate into one large deposit (Sputnik Planitia) owing to lower-albedo terrains that surround the higher-albedo ice. The darker terrains have higher surface temperatures, resulting in an enhancement of volatile ice sublimation from the margins of the ice deposits. Thus, if ice condensation is constant across the interiors of multiple ice sheets, then smaller ice sheets experience a larger fractional loss of ice from their margins, resulting in their eventual disappearance and atmospheric transport of their volatile content to a single dominant ice deposit (a process we term 'oligarchic growth of cold traps').

If reorientation is controlled by the accumulation of volatiles within Sputnik Planitia, then the approximate reorientation timescale can be estimated from the time required to fill Sputnik Planitia with volatiles. From Fig. 2b and Extended Data Fig. 3, the typical volatile ice thicknesses required to drive reorientation are around 5 km. Following ref. 35, it would take approximately 5 million years to grow a 5 km N_2 ice cap given Pluto's present average atmospheric pressure and temperature[33].

Similar timescales can be estimated by considering sublimation mass fluxes due to seasonal differences in insolation[7].

Seasonal wobbles of Pluto due to mass transport into and out of Sputnik Planitia. If volatiles migrate into and out of Sputnik Planitia on seasonal timescales, then one may expect corresponding small-scale oscillations in the planet's principal axes of inertia. These small-amplitude wobbles would be analogous to atmospheric-pressure-driven wobbles on Earth[25]. Extended Data Fig. 8a, b shows how Pluto's minimum and maximum principal axes of inertia would change orientation in response to small changes in the thickness of volatile ices within Sputnik Planitia. If these changes occurred seasonally, then Pluto would not have time to damp the tidal rotational energy (TPW timescales are generally of the order of millions of years), and the principal axes would wobble about the tidal and rotational axes[25,36]. In a reference frame fixed to Pluto, such wobbles would result in apparent motions of Pluto in the sky (even though Pluto and Charon would remain in almost perfect double synchronous spin–orbit lock). Such motions would result in tidal heating very similar to obliquity and/or libration tides, which can be important for the heat budget of icy satellites[37]. Because these wobbles are driven by the continual sublimation and redeposition of volatiles on Pluto, they may be persistent, resulting in small but continual amounts of extra heating within Pluto.

The amount of heat generated from these postulated seasonal wobbles can be estimated by determining the change in rotational kinetic energy in response to the transport of ice into and out of Sputnik Planitia. Rotational kinetic energy, KE, is related to the planet's spin vector, $\boldsymbol{w}$, and its inertia tensor, I: $\mathrm{KE} = \boldsymbol{w}^{\top}\boldsymbol{I}\boldsymbol{w}$. For Pluto's current rotation rate (6.39 Earth days), and typical assumptions of Pluto's figure and moments of inertia (described above), Pluto's rotational kinetic energy is about 4.7×10^{23} J. Adding or removing one metre of ice (approximately the amount of ice transported seasonally across Pluto[7]) from Sputnik Planitia changes this rotational kinetic energy by approximately 10^{17} J (assuming the rotation rate remains unchanged) (Extended Data Fig. 8c). Assuming this occurs over one Pluto year (248 Earth years), this translates into a heat production rate of 5×10^{7} J s^{-1}. This is approximately 1/1,000 of the present-day radiogenic heating expected within Pluto[38]. Although the expected heat production rate is low, this heat may be released closer to the surface (for example, localized in crustal faults), whereas radiogenic heating is probably concentrated within Pluto's silicate core, deep beneath the surface. Future work will need to quantify the mechanics and efficacy of this 'wobble-heating' process in more detail.

The magnitude and geometry of any such wobbles depend on both the amount of material being transported and the differences between Pluto's moments of inertia (equivalently, its degree-2 spherical harmonic gravity coefficients[27]). If the TPW hypothesis for Sputnik Planitia is correct, then Pluto's present-day degree-2 gravity has some contributions from Sputnik Planitia and Pluto's reoriented remnant figures. The exact values depend on the proposed reorientation event. Extended Data Fig. 8d–f shows predicted, present-day spherical harmonic gravity coefficients for the reorientation geometries summarized in Fig. 2a. Future measurement of degree-2 gravity of Pluto, be it from spacecraft or remote observations of wobbles, may further constrain which TPW models for Sputnik Planitia are viable.

Other geologic evidence for reorientation. Sublimation often creates geologic features that align north–south. Although several terrains on Pluto are characterized by elongated, plausibly sublimation-driven landforms (for example, pitted uplands and the bladed terrain of Tartarus Dorsa[2]), not all align north–south. The washboard terrain northwest of Sputnik Planitia is characterized by parallel ridges and troughs that trend southwest–northeast[2]. In our pre-TPW view of Pluto, these features become aligned north–south (Extended Data Fig. 4a, b). Relative age-dating of these features and other sublimation structures may provide constraints on the timing of the formation of Sputnik Planitia.

If the reorientation of Pluto was due to the gradual infill of volatiles within Sputnik Planitia (as in Fig. 3d–i), then the stress and tectonic patterns may also change gradually with time. The time evolution of the tectonic patterns predicted by our simple reorientation model (Fig. 3d–i) are shown in Extended Data Fig. 6 and Supplementary Videos 1–3. A nearly ubiquitous result in these tectonic models is that at a certain distance away from Sputnik Planitia, faults transition from being quasi-radial to Sputnik Planitia to quasi-azimuthal. This transition marks a change in the dominant source of stress; loading stresses dominate near Sputnik Planitia, whereas reorientation stresses dominate far away. We use this transition as evidence of the reorientation to explain the sharp change in fault azimuths observed on Pluto (Fig. 2g–k). Curiously, the location of this transition changes as a function of the loading within Sputnik Planitia in these time-sequence models. In particular, the transition moves progressively further away from Sputnik Planitia as it is filled with volatiles (Extended Data Fig. 6a–f). Eventually, for very thick deposits within Sputnik Planitia, the loading stresses dominate reorientation stresses globally (Extended Data Fig. 6g, h). This change in stress field with time may be recorded in the cross-cutting relationships of faults on Pluto. For example, we may predict that within the faults far from Sputnik Planitia (Djanggawul and the 'spider'), faults closer to Sputnik Planitia will be older, and may be cross-cut by faults radial to Sputnik Planitia. Further geologic mapping of Pluto (even in regions far from Sputnik Planitia), may provide valuable insight into the nature and origin of Sputnik Planitia.

The mass anomaly and underlying structure of Sputnik Planitia. As noted in the main text, the mass anomaly from a 3-km-deep, uncompensated topographic depression has a mass anomaly of $Q' = -4.14$ (Fig. 2b), which is too large and negative for Sputnik Planitia to be at its present location. Sputnik Planitia must have a mass anomaly between -0.3 and 1.8 to be at its present location. With $Q' = -4.14$, Sputnik Planitia would reorient almost completely to the north pole. Adding volatiles into the basin (while maintaining a 3-km-deep basin) reduces the mass anomaly of the basin. However, for typical values for the density of the Pluto's ice-rich crust (930 kg m^{-3}) and the predominantly N_2 volatile ice within the basin (1,000 kg m^{-3}), the thickness required to give $-0.3 < Q' < 1.8$ is well above the estimated thickness of the volatile ice (<10 km; refs 2, 4, 5). Although decreasing the density of the crust and increasing the density of the volatile infill can reduce the required thickness (Extended Data Fig. 3b), it is difficult (it would require a very dense volatile infill and extremely low-density crust). Thus, for Sputnik Planitia to be at its present location, the underlying basin must at least be partially compensated.

If Sputnik Planitia is an impact basin, then there are several processes that could plausibly compensate for the mass anomaly associated with the topographic depression. These processes can include mantle uplift, isostatic adjustment of the basin and surrounding terrains, cooling and contraction of impact melt, changes in porosity and the emplacement of ejecta[15]. On the Moon and other terrestrial planets, these processes often give impact basins stochastically positive and negative total mass anomalies, despite being topographic lows (Extended Data Fig. 1; ref. 12). Even if impact processes on icy planets and satellites are somehow fundamentally different than those on their terrestrial counterparts, unavoidable components such as ejecta blankets can considerably offset the negative mass anomaly from the topographic depression. This may be why large impact basins on other icy bodies do not always result in poleward reorientation (for example, Herschel on Mimas[17]). As an example, the reorientation of the Moon due to the formation of the South Pole–Aitken impact basin was more strongly controlled not by the basin itself, but by the deposition of a thick ejecta blanket on the far side of the Moon[12,39].

Extended Data Fig. 3 showcases four possible simple structures for the Sputnik Planitia basin, and their impact on its total mass anomaly. The first model (Extended Data Fig. 3a) looks at volatiles loading an underlying basin that has an intrinsic mass anomaly of $Q' = 0$, which is dynamically equivalent to volatiles loading the surface of the planet. Since the Q' value of mass anomalies on other planets is seemingly random (Extended Data Fig. 1; ref. 12), this model serves as our null hypothesis, and is what we use to estimate ice thicknesses for loading and tectonic calculations. The second model (Extended Data Fig. 3b) considers ice filling a basin of fixed depth, and is already discussed above. The third model (Extended Data Fig. 3c) is a simple impact basin model (based on ref. 40) consisting of ice filling a basin of fixed depth, surrounded by an ejecta blanket with a total volume set by the total amount of material excavated from within the basin. The final model (Extended Data Fig. 4d) consists of a basin that is initially isostatically compensated by an uplift in a subsurface ocean, and subsequently filled with volatiles. This final model is examined more thoroughly in refs 16 and 41. Additional models can be constructed by summing components from the mass anomaly menu in Extended Data Fig. 2.

The inclusion of an ejecta blanket substantially offsets the mass anomaly associated with the topographic low of the Sputnik Planitia basin—from $Q' \approx -4$ to $Q' \approx -2$ (Fig. 2b, Extended Data Fig. 3c). This is still too negative for Sputnik Planitia to be at its present location (requiring $0.3 < Q' < 1.8$). Thus, like the model without ejecta (Extended Data Fig. 3b), this then requires that Sputnik Planitia must have some extra positive mass anomaly contributing to its total mass anomaly. However, including impact ejecta enables the volatiles within the basin to play a much larger role in the total mass anomaly for three reasons. First, adding an ejecta blanket changes the depth of the basin with respect to the mean radius of Pluto; we assume that the depth of the basin is measured with respect to the crater rim. Second, by reducing the mass anomaly of the underlying basin, it reduces the amount of volatiles required within the basin to reach an acceptable Q' value. Lastly, as the thickness of the volatiles within the basin increases, the total excavated volume of Sputnik Planitia increases, thus increasing the thickness of ejecta blanket. This results in steeper curves for Q' as a function of volatile ice thickness in Extended Data Fig. 2c compared with Extended Data Fig. 2b. Taking the ejecta blanket into account reduces the required volatile ice thickness from tens or hundreds of kilometres from the simple basin model (Extended Data Fig. 2b) to less than 10 km, which is consistent with other estimates for the thickness of volatiles within Sputnik Planitia[2,4,5]. If the thickness of volatiles within Sputnik Planitia is larger, then Sputnik Planitia must have an additional negative mass anomaly to enable it to be at its present location.

The inclusion of an uplift in the postulated subsurface ocean results in a similar Q' value to models with an ejecta blanket. If the initial (pre-volatile filled) Sputnik Planitia basin is isostatically compensated (via Airy isostasy), then the initial mass anomaly of the basin reduces from $Q' \approx -4$ to $Q' \approx -2$ (Fig. 2b, Extended Data Fig. 3d). It is important to note that despite the fact that this initial basin is 'compensated' it does not have $Q' = 0$. This arises from how a compensated structure fundamentally alters the inertia tensor (and thus Q'). Because the structure compensating for the topographic low is deeper within the planet, it contributes less to the inertia tensor (inertia tensors scale with radial distance squared), and thus the negative mass anomaly arising from the topographic low still dominates. Nonetheless, this reduction of the underlying basin's Q' value is sufficient to allow volatiles to overcome the remaining negative mass anomaly for ice thicknesses of 1–10 km. This mechanism is discussed much more rigorously in ref. 16. Continued study of New Horizons data, as well as thorough impact simulation studies, is needed to truly disentangle the possible cause of the positive mass anomaly within Sputnik Planitia.

26. Arfken, G. B. & Weber, H. J. *Mathematical Methods for Physicists* 7th edn 797–798 (Academic, 1995).
27. Lambeck, K. *The Earth's Variable Rotation: Geophysical Causes and Consequences* (Cambridge Univ. Press, 1980).
28. Takeuchi, H. & Saito, M. in *Methods in Computational Physics* (ed. Bolt, B. A.) 217–295 (Academic Press, 1972).
29. Sabadini, R., Vermeersen, B. & Cambiotti, G. *Global Dynamics of the Earth: Applications of Viscoelastic Relaxation Theory to Solid-Earth and Planetary Geophysics* (Springer, 2016).
30. Wahr, J. *et al.* Modeling stresses on satellites due to nonsynchronous rotation and orbital eccentricity using gravitational potential theory. *Icarus* **200,** 188–206 (2009).
31. Anderson, E. M. *The Dynamics of Faulting* (Oliver & Boyd, 1951).
32. Schenk, P., Matusyama, I. & Nimmo, F. True polar wander on Europa from global-scale small-circle depressions. *Nature* **453,** 368–371 (2008).
33. Gladstone, G. R. The atmosphere of Pluto as observed by New Horizons. *Science* **351,** aad8866 (2016).
34. Bertrand, T. & Forget, F. Observed glacier and volatile distribution on Pluto from atmosphere–topography processes. *Nature* http://dx.doi.org/10.1038/nature19337 (2016).
35. Langmuir, I. The vapor pressure of metallic tungsten. *Phys. Rev.* **2,** 329–342 (1913).
36. Spada, G., Sabadini, R. & Boschi, E. Long-term rotation and mantle dynamics of the Earth, Mars, and Venus. *J. Geophys. Res.* **101,** 2253–2266 (1996).
37. Nimmo, F. & Spencer, J. R. Powering Triton's recent geologic activity by obliquity tides: implications for Pluto geology. *Icarus* **246,** 2–10 (2015).
38. McKinnon, W. B., Simonelli, D. P. & Schubert, G. in *Pluto and Charon* (eds Stern, S. A. & Tholen, D. J.) 295–346 (Univ. Arizona Press, 1997).
39. Kendall, J. D., Johnson, B. C., Bowling, T. J. & Melosh, H. J. Ejecta from south pole-Aitken basin-forming impact: dominant source of farside lunar highlands. In *46th Lunar Planet. Sci. Conf.* 2765 (Lunar and Planetary Institute, 2015).
40. Melosh, H. J. Large impact craters and the Moon's orientation. *Earth Planet. Sci. Lett.* **26,** 353–360 (1975).
41. Johnson, B. C., Bowling, T. J. Trowbridge, A. J. & Freed, A. M. Formation of the Sputnik Planum basin and the thickness of Pluto's subsurface ocean. *Geophys. Res. Lett.* **43,** 10068–10077 (2016).

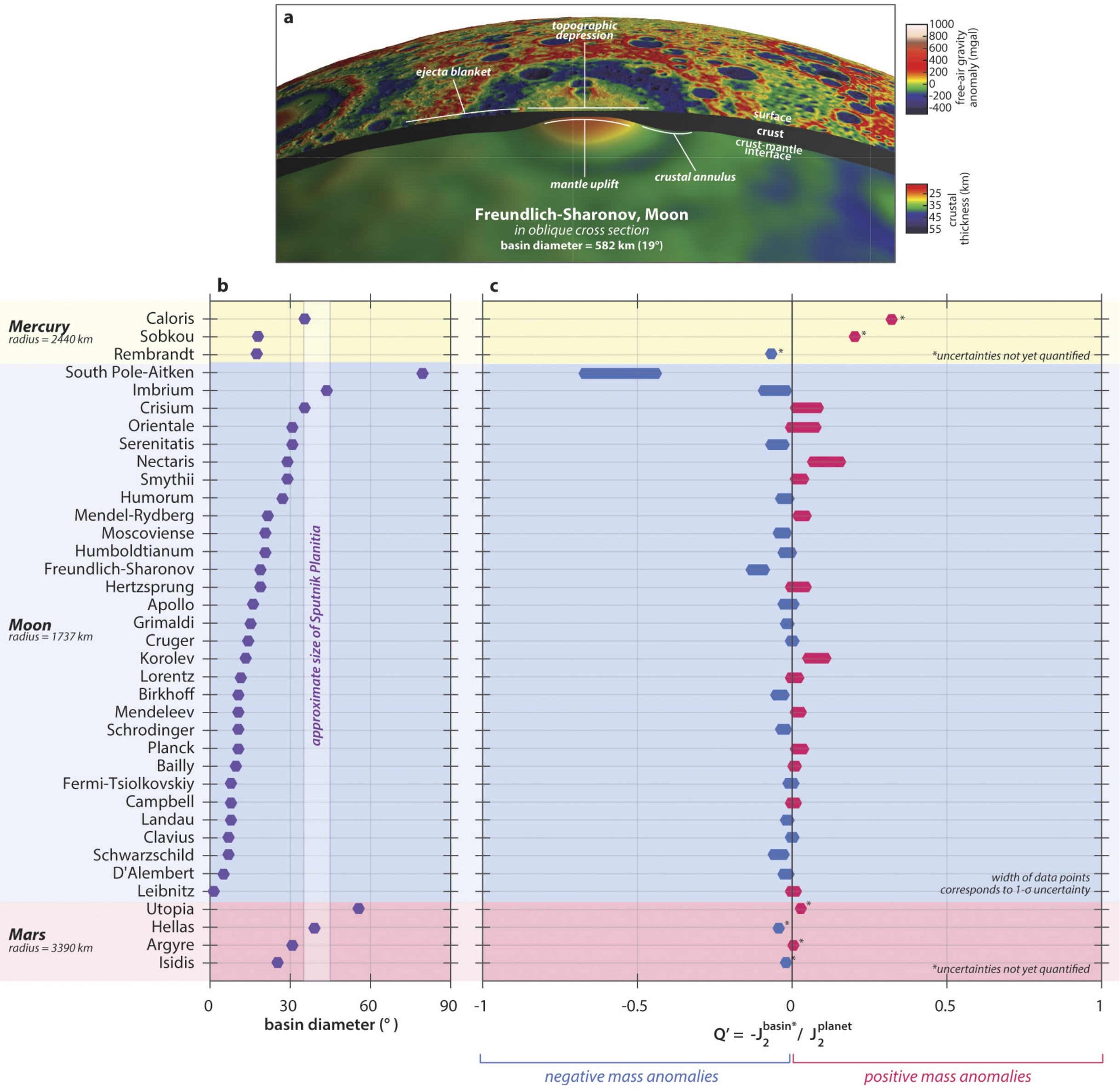

Extended Data Figure 1 | Mass anomalies of impact basins on other planetary bodies. a, An oblique cross-section of a typical lunar mascon basin, Freundlich–Sharonov, highlighting the different components that contribute to a basin's overall mass anomaly. **b**, A table of large basins on other planetary bodies (in order of the basin's diameter relative to the host planet) for which we have adequate gravity measurements to determine their respective mass anomalies. **c**, The mass anomaly of each basin. The mass anomalies for lunar impact basins have been comprehensively characterized in ref. 12. Mass anomalies for impact basins on Mars and Mercury are calculated in the same way, using available gravity data for these two bodies. Uncertainties have not been quantified for impact basins on Mars and Mercury.

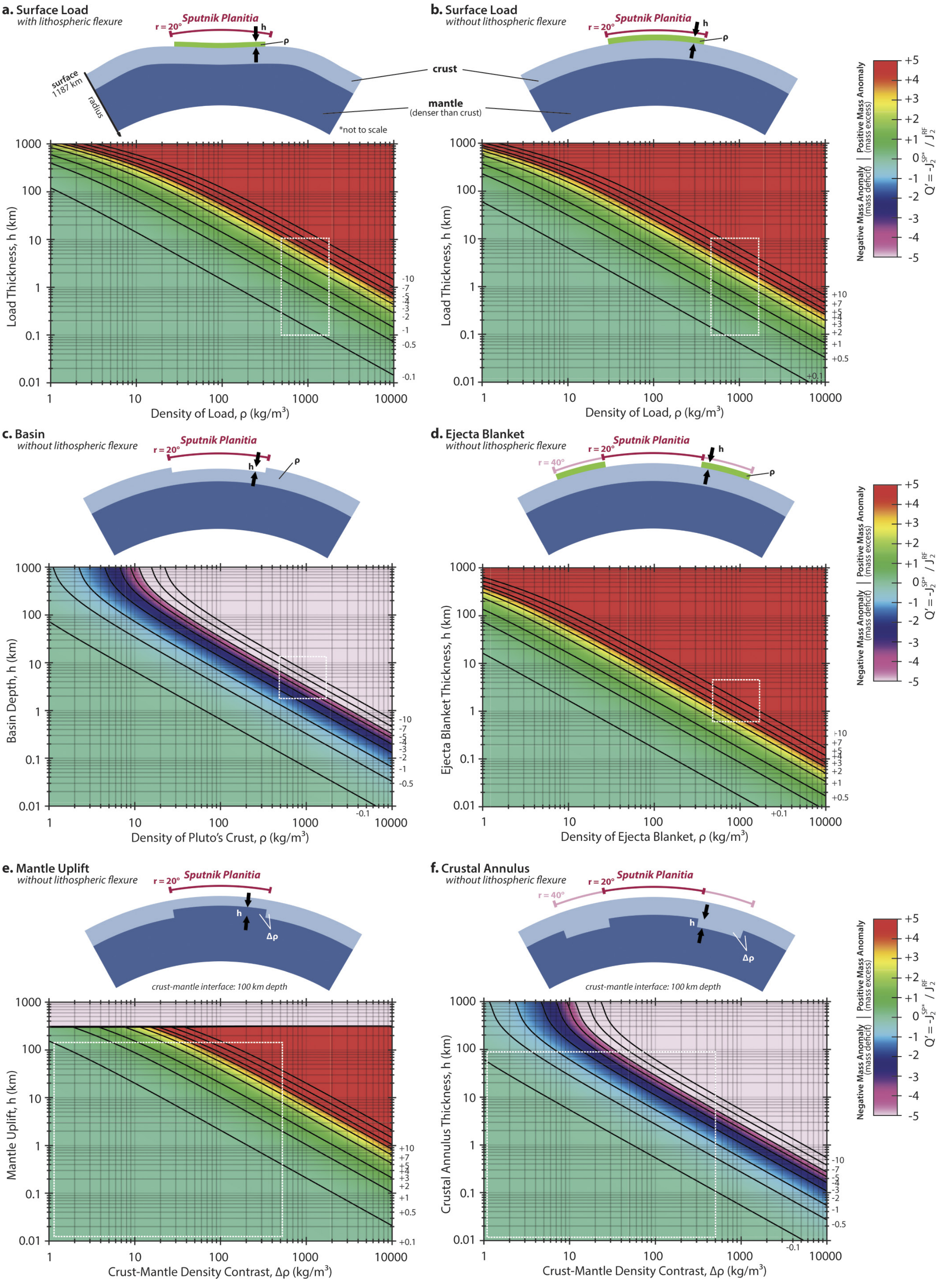

Extended Data Figure 2 | Mascon components and their mass anomalies. a–f, Mass anomaly (Q') of an individual component of a basin (for example, volatile ice load or topographic depression) as a function of that component's thickness and density. White dashed regions denote plausible areas of parameter space (densities of ices on Pluto are from ref. 7; basin depths and ice thicknesses are from refs 1, 2, 4, 5; ejecta blanket thicknesses are estimated by redistributing the mass excavated from the basin into an annulus outside the basin, between 1 and 2 crater radii). The mass anomaly of the impact basin can be constructed by linearly summing these components.

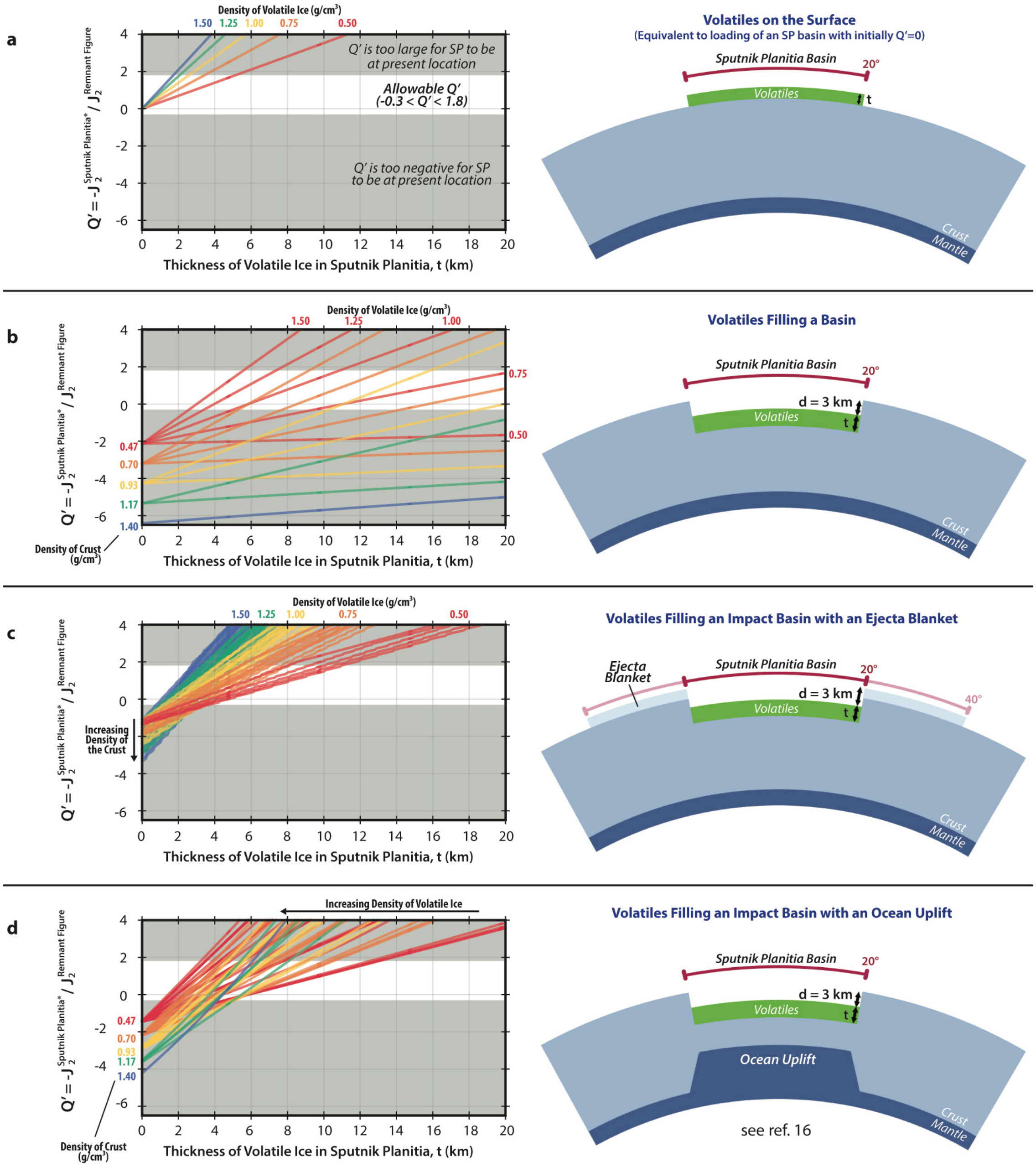

Extended Data Figure 3 | Simple models for Sputnik Planitia. a–d, Q' as a function of volatile thickness (left column) for each simple model of Sputnik Planitia (right column). Different colours and lines denote different model results assuming different densities of model components (volatile ice density, crust density, mantle density, and ejecta density, when appropriate). Nominal outputs from each model are shown in Fig. 2b. See Methods for discussion of this figure. **a**, Volatiles loading on the surface of a planet, which is equivalent to volatiles loading a basin with no intrinsic mass anomaly. **b**, Volatiles filling an initially uncompensated basin, with a fixed depth of 3 km from the surface of the planet to the top of the volatiles. **c**, Volatiles filling an initially uncompensated impact basin surrounded by an ejecta blanket extending from 1 to 2 crater radii containing the total mass excavated from within the basin. The height from the top of the rim to the top of the volatiles is fixed to 3 km. **d**, Volatiles filling a basin that is initially compensated from isostatic uplift of the presumed ocean at depth (see ref. 16 for a more thorough investigation of this hypothesis). In all plots, it is assumed that volatiles are partially supported by Pluto's elastic lithosphere (Methods).

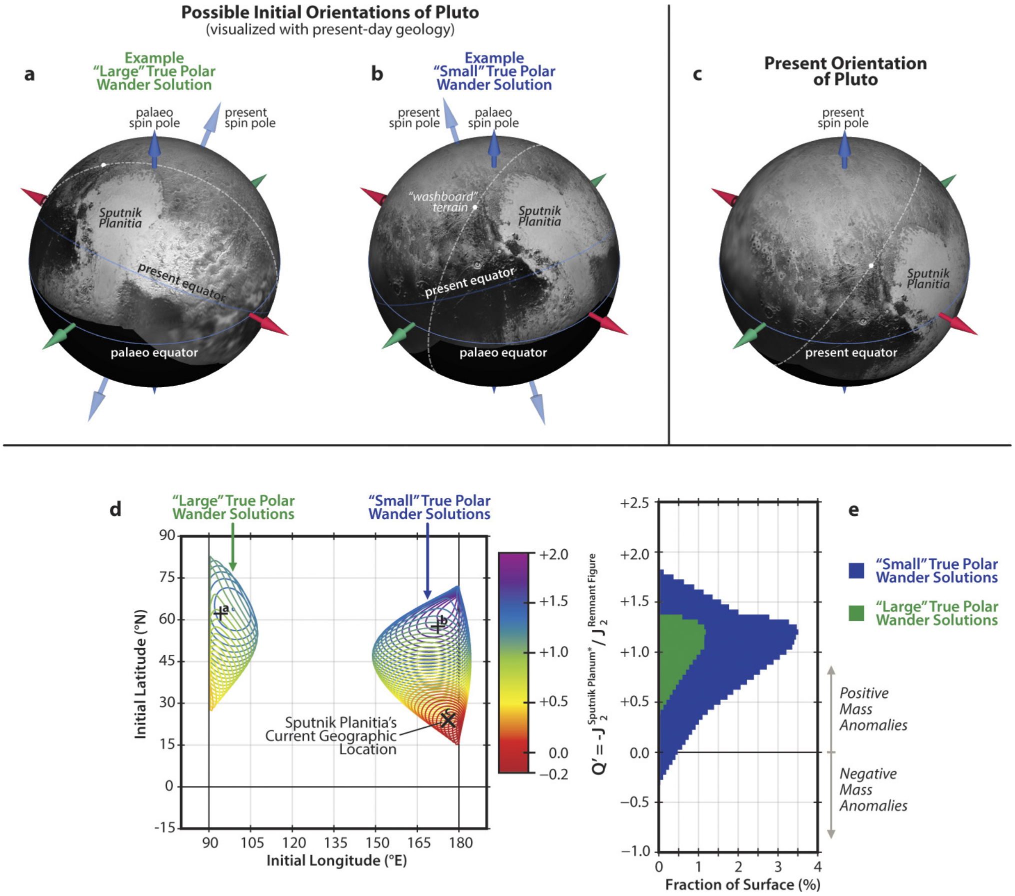

Extended Data Figure 4 | The initial orientation of Pluto and the range of possible mass anomalies. a–**c**, Orthographic spherical projections of Pluto for example initial orientations from the perspective of an inertial viewer, fixed with respect to the tidal/rotational axes. Base map: NASA/Johns Hopkins University Applied Physics Laboratory/Southwest Research Institute. The dashed white line indicates the strike of the 'washboard terrain' (Methods). **d**, Contours enclosing the possible initial locations of Sputnik Planitia as a function Q'. This is the same as Fig. 2a, but in an equirectangular map projection. **e**, Histogram of the Q' values of allowable reorientation scenarios as shown in **d** (and Fig. 2a). The vast majority of solutions are positive mass anomaly solutions.

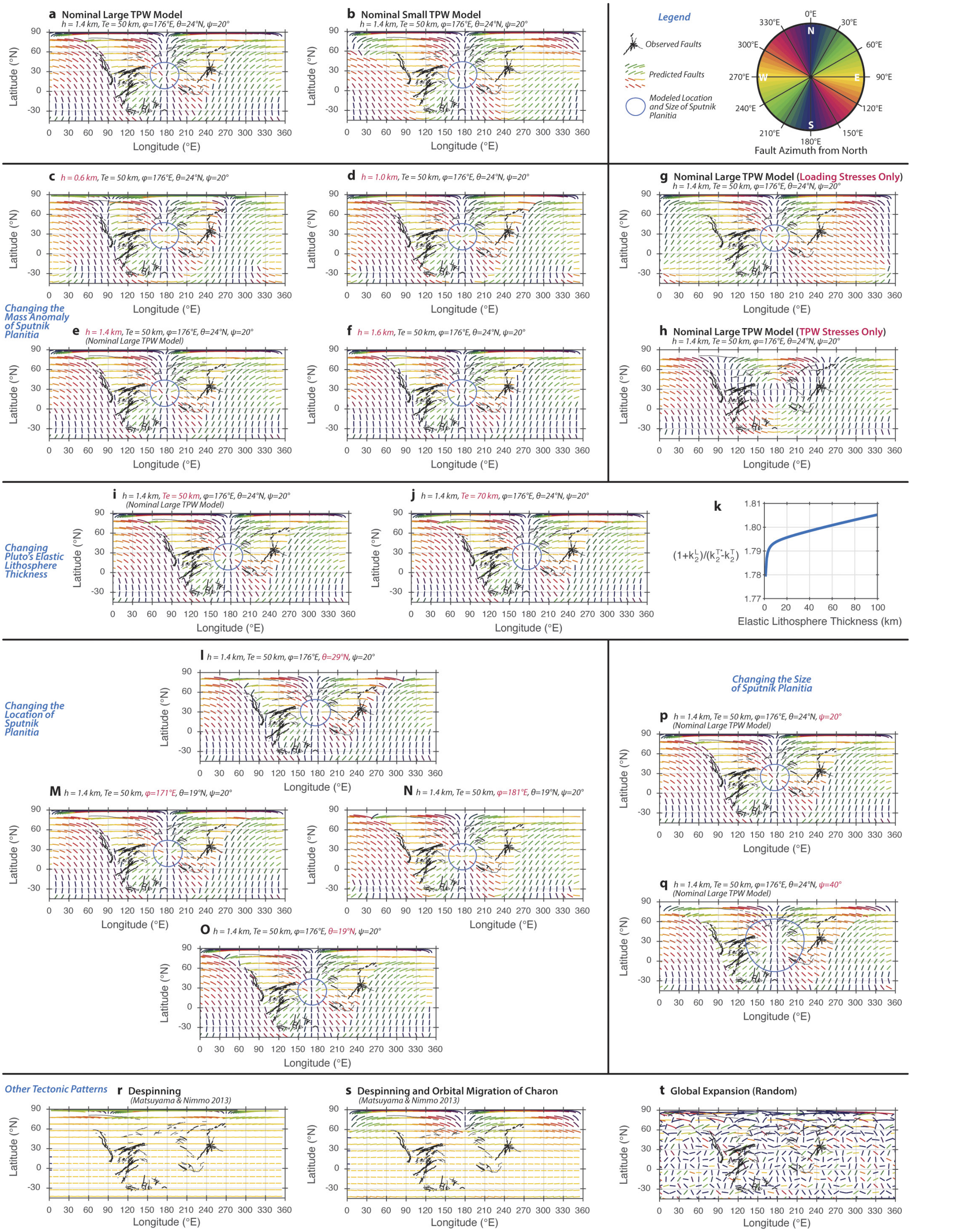

Extended Data Figure 5 | Tectonic models. a–q, Tectonic patterns depend on the geometry of proposed reorientation (**a–f**), the interior structure (**i–k**), and the size and location of the perturbing load (**l–q**). Yet, despite all of the possible dependencies, it is striking that for the allowed reorientation scenarios, the predicted tectonic patterns show little variance. Most predict quasi-radial faults proximal to Sputnik Planitia (due to loading, **g**), transitioning to quasi-azimuthal faults distal to Sputnik Planitia (due to TPW stresses, **h**). Faults are coloured by azimuth, as in Fig. 2g–j. Black lines show mapped faults, as in Fig. 2g, h. **r–t**, Tectonics patterns from TPW, loading and global expansion provide a far better match to the observed fault distribution than do de-spinning, orbit migration or global expansion.

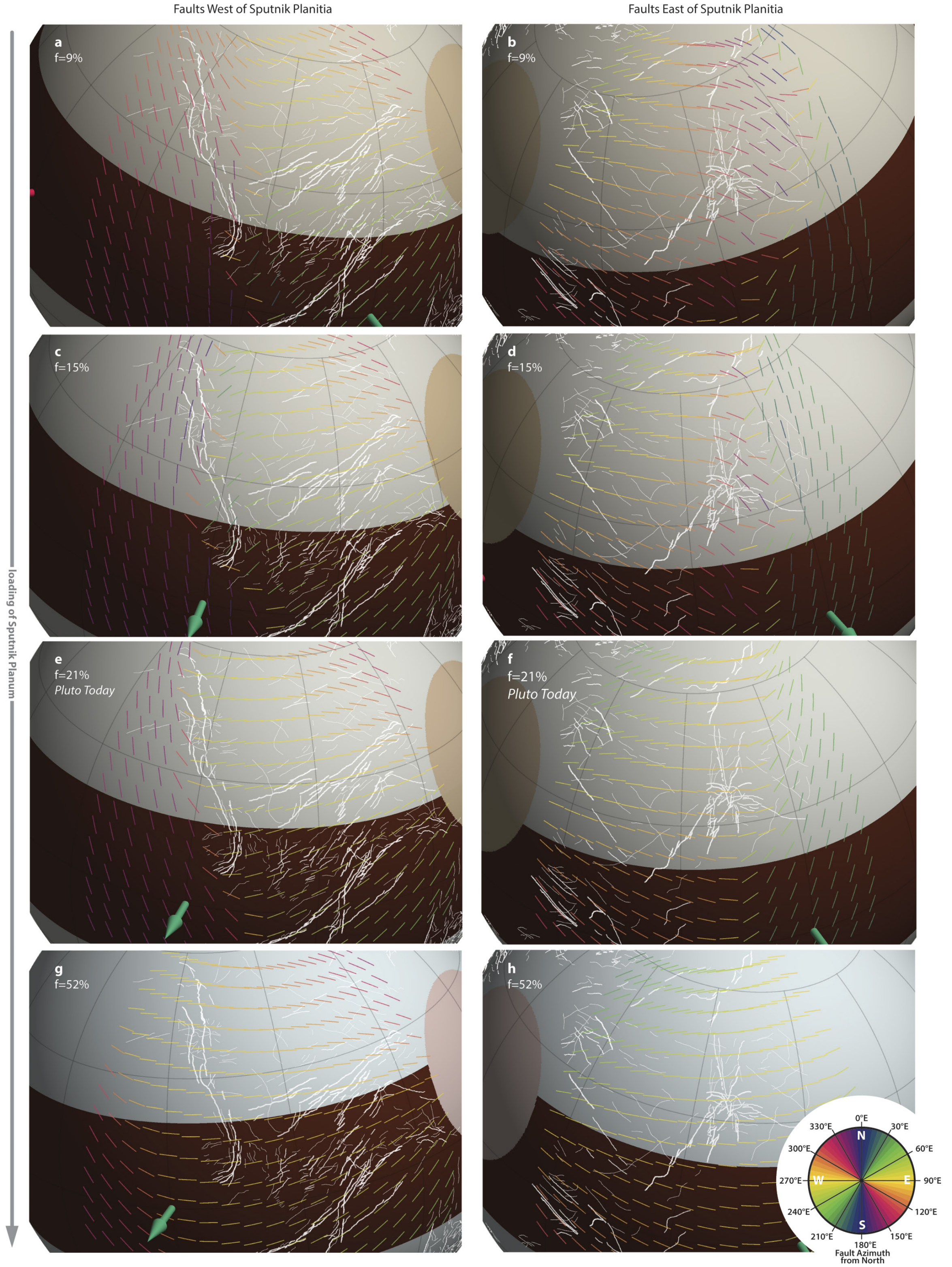

Extended Data Figure 6 | Tectonics due to the progressive loading of Sputnik Planitia. a–h, The predicted tectonic pattern on Pluto as a function of the amount of ice within Sputnik Planitia, as in Fig. 3d–i: *f* denotes the fraction of the total global reservoir of ice within Sputnik Planitia (where the reservoir is equivalent to a 200-m-thick global layer); $f=9\%$ corresponds to 500 m, $f=12\%$ corresponds to 800 m (as in Fig. 3f), $f=21\%$ corresponds to 1,400 m (as in Fig. 3g) and $f=52\%$ corresponds to 3,500 m. The left column shows a view above the faults west of Sputnik Planitia, while the right column shows a view above the faults east of Sputnik Planitia. Grid lines and coloured vectors denote the instantaneous principal axis reference frame. As Sputnik Planitia is loaded with volatiles, Pluto reorients. This changes the location of these features with respect to the principal axis reference frame (resulting in the reorientation of the latitude and longitude grid in each frame). This also changes the stresses as a function of loading within Sputnik Planitia, resulting in time-evolution of the tectonic patterns. The transition from quasi-radial (loading-dominated) to quasi-azimuthal (TPW-dominated) faults increases in distance from Sputnik Planitia as a function of the loading within Sputnik Planitia. This change in stress pattern may be reflected in future study of the cross-cutting relationships of Pluto's faults. These images are snapshots from Supplementary Videos 1–3, which show additional time-steps.

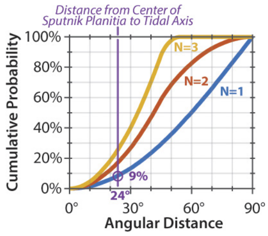

Extended Data Figure 7 | Probability of randomly being near a principal axis. The probability of a randomly located feature being located near to any given principal axis (or set of axes). *N* is the number of axes considered; for example, the blue line indicates the chance probability of being near any single principal axis, whereas the yellow line indicates the chance probability of being near any of the principal axes. There is a 9% probability of Sputnik Planitia being this close to the tidal axis of Pluto.

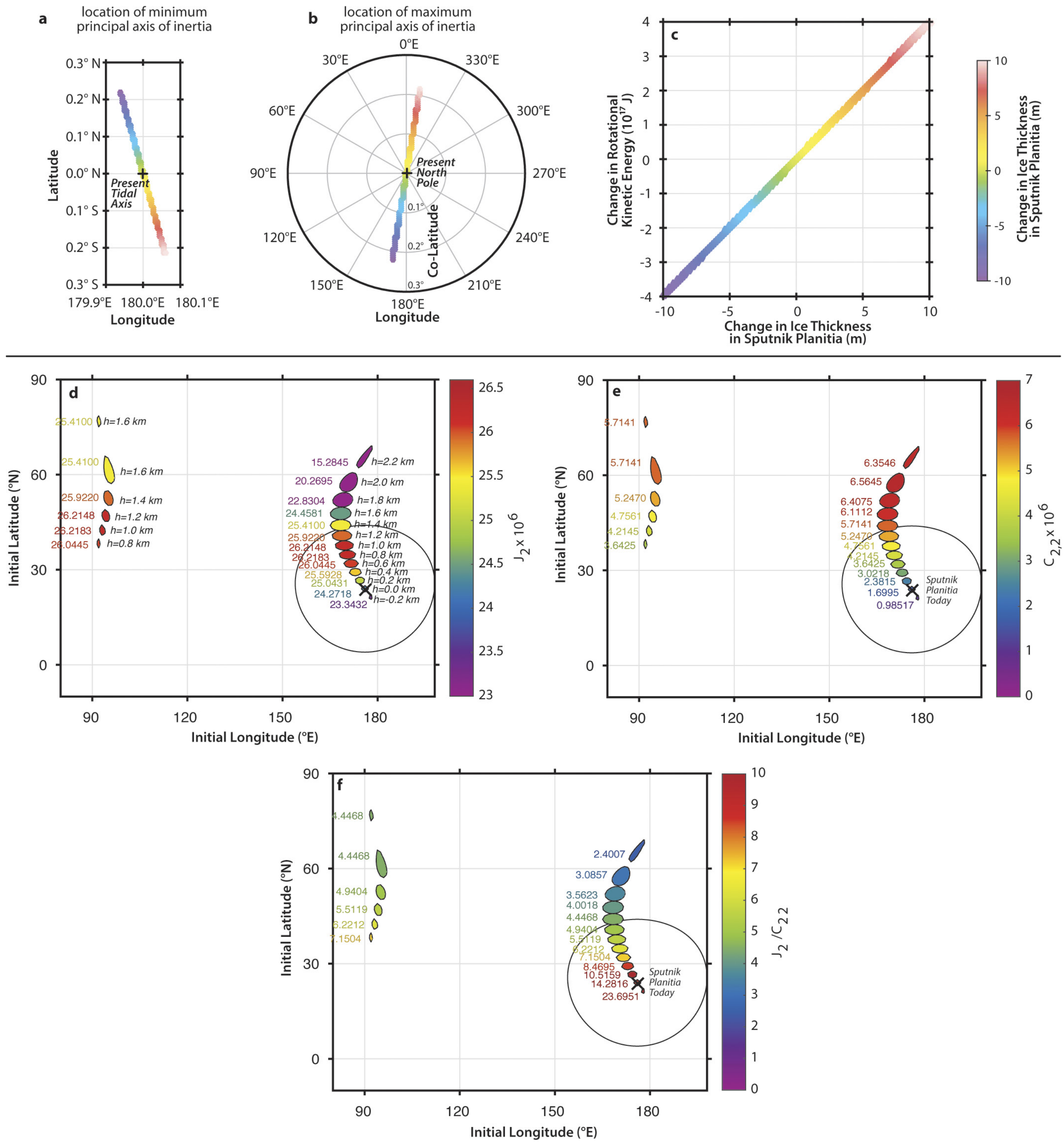

Extended Data Figure 8 | Pluto's wobbles. a, **b**, The location of Pluto's minimum (**a**) and maximum (**b**) principal axes of inertia with respect to their present locations as a function of changes in ice thickness in Sputnik Planitia. Around 1 m of volatile ice can be transported seasonally across the entire surface of Pluto[7], although it is unclear how volatiles migrate into and out of Sputnik Planitia. **c**, The change in rotational kinetic energy resulting from the transport of volatile ice into and out of Sputnik Planitia. **d**–**f**, The spherical harmonic degree-2 gravity coefficients associated with Sputnik Planitia and the remnant figure for each of the possible reorientation scenarios shown in Fig. 2a. Measurements of degree-2 gravity (or equivalently the moments of inertia) of Pluto will constrain possible reorientation scenarios.